Journal of Structural Geology 116 (2018) 131–145

Contents lists available at ScienceDirect

Journal of Structural Geology

journal homepage: www.elsevier.com/locate/jsg

Strain analysis of the Xuefengshan Belt, South China: From internal strain variation to formation of the orogenic curvature

Yang Chu[a,b,*], Wei Lin[a,b]

[a] State Key Laboratory of Lithospheric Evolution, Institute of Geology and Geophysics, Chinese Academy of Sciences, Beijing, 100029, China
[b] University of Chinese Academy of Sciences, Beijing, 100049, China

ARTICLE INFO

Keywords:
South China
Xuefengshan belt
Finite strain
Strain gradient
Orogenic curvature

ABSTRACT

The Early Mesozoic Xuefengshan Belt, located in the central part of the South China Block, East Asia, developed as an intracontinental belt during the Middle Triassic. Analyses of structural and strain patterns in Neoproterozoic conglomerates constrain the internal deformation and three-dimensional kinematic evolution of this fold-and-thrust belt. Finite strain data (R_{XZ}) range from 1.1 to 3.2 and generally increase eastwards towards the deep units of the orogenic core. Our results also show that at basal décollement zone the D_1 schistosity-forming deformation has a gradient of stronger fabrics, higher strain ratios, and a dominant thrust-normal flattening mechanism. High tectonic levels exhibit lower strain ratios and later structural overprinting that locally modified the D_1 strain patterns. Parallel to the belt, enhanced strain and tectonic uplifting along the northern and southern sections of the belt indicate an along-strike structural variation that corresponds to the formation of the orogenic curvature. During the thrusting propagation, large igneous intrusions escaped deformation due to their stiffness and facilitated strain accumulation on the peripheries, whereas stress in the central part migrated progressively and formed a tectonic salient towards the west without significant strain localization.

1. Introduction

When rigid tectonic blocks are subjected to horizontal contraction, a linear fold-and-thrust belt is formed at their margins as one of the most complex and significant tectonic units on Earth. Tectonic belts resulting from different tectonic settings often demonstrate distinctive structural patterns. Thus, a thorough investigation on deformation pattern is necessary to reveal both the geologic history and regional stress regimes. In detail, structural fabrics and strain data are regarded as key information for further structural analysis, and the quantification of deformation can greatly improve structural geology in understanding rock rheology and behavior during progressive deformation (Erslev, 1988; Kenis et al., 2005; Yonkee and Weil, 2010). Nevertheless, structures at multiple scales may reflect different information for quantification. For example, balanced cross-sections provide shortening estimation based on information from kilometer-scale regional thrusts and folds, and strain measurements are closely dependent on micro-scale to hand specimen-scale analysis (Ramsay and Huber, 1983; Lisle, 1985). In order to understand the entire history of a fold-and-thrust belt, strain is critical to evaluate the internal deformation pattern that may deviate from bulk deformation (Mitra, 1994).

Quantitative strain data constitute an important aspect of deformation in orogenic belts, and can provide clues for determining spatial-temporal distribution of rock units and processes responsible for tectonic evolution. Due to heterogeneity, differential deformation give rise to various structural modes of fold-and-thrust belts, and deserves careful strain examination (Mitra, 1994; Long et al., 2011). As a good indicator, sheared sedimentary rocks, such as conglomerates, have long been used to constrain finite strain and to evaluate features of internal deformation in different geodynamic settings (Mukul and Mitra, 1998; Kirkland et al., 2006; Long et al., 2011; Tull et al., 2012). In South China, the Xuefengshan Belt forms as an intracontinental orogen in the central portion of the South China Block, and records polyphase deformation. Although the architecture of this belt has been well documented (Yan et al., 2003; Wang et al., 2005; Chu et al., 2012a, 2012b), information on internal strain patterns and how they evolved in the intracontinental setting remain less understood. Across the whole belt, a thick layer of conglomerate and sandstone of Neoproterozoic deposition age is well exposed and intensively sheared, providing a natural laboratory for strain estimation. In this study, quantitative strain data allow us to reveal the strain variation of the Xuefengshan Belt, and then to discuss the geometry and evolution of this intracontinental belt.

* Corresponding author. Institute of Geology and Geophysics, Chinese Academy of Sciences, 19 Beituchengxi Road, Chaoyang District, 100029, Beijing, China.
E-mail address: chuyang@mail.iggcas.ac.cn (Y. Chu).

https://doi.org/10.1016/j.jsg.2018.08.002
Received 9 December 2017; Received in revised form 2 August 2018; Accepted 2 August 2018
Available online 10 August 2018
0191-8141/

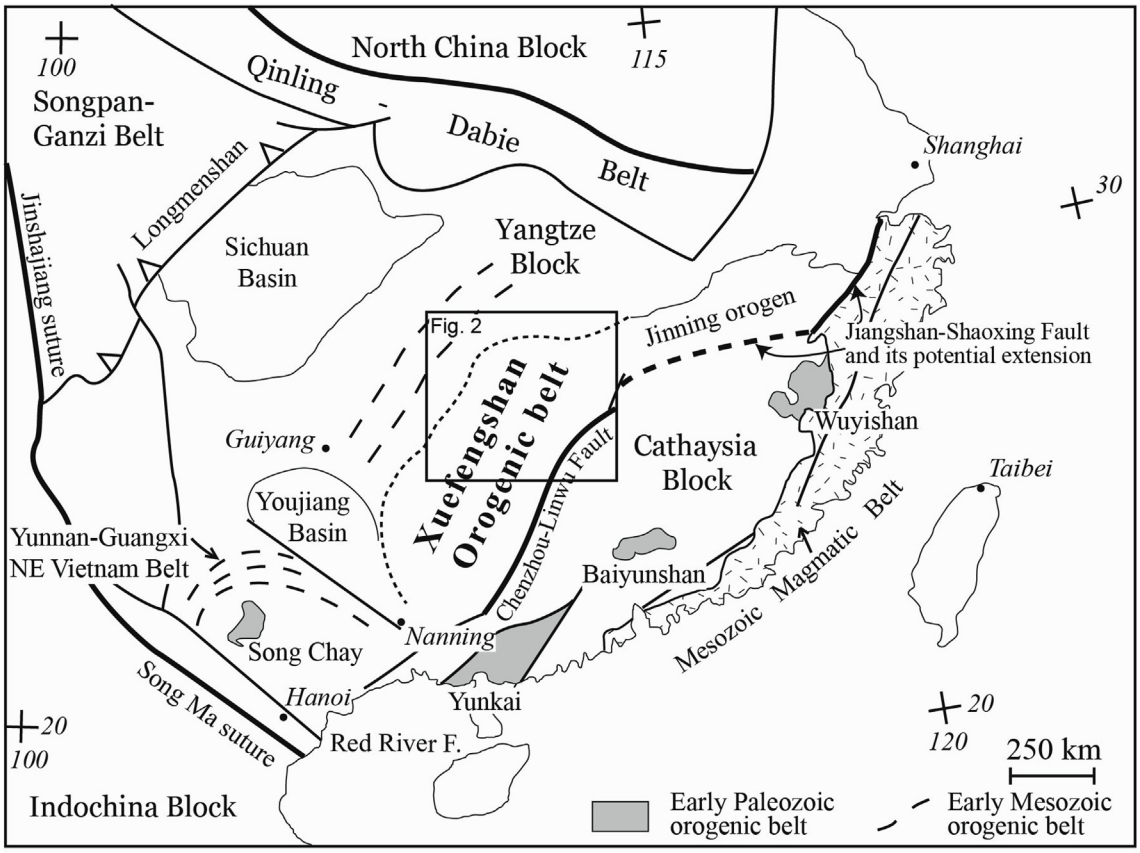

Fig. 1. Tectonic sketch map of South China (Modified after Faure et al., 2009). Early Mesozoic peripheral orogens of the South China Block are indicated on the map. The South China Block is subdivided into the Yangtze Block to the west, and the Cathysia Block to east, both of which were involved in Triassic intracontinental deformation. The crosses with numbers on the map indicate the longitude and latitude.

2. Geological setting

2.1. Tectonic evolution of the South China block

The amalgamation of the South China Block (SCB) occurred in the Neoproterozoic, following the collision between the Yangtze Block and the Cathaysia Block (Fig. 1), and produced the Jiangnan orogenic belt with intense crustal shortening, ophiolite emplacement, and post-orogenic magmatism (Charvet et al., 1996; Shu and Charvet, 1996; Li et al., 2003; Wang et al., 2013). However, this event was concealed by the Paleozoic sedimentary cover or large-scale modification by Early Paleozoic intracontinental reworking (Wang and Li, 2003; Faure et al., 2009; Charvet et al., 2010; Li et al., 2010, 2016; Chu and Lin, 2014).

From Late Permian to Triassic, the SCB was confined and intensely modified by peripheral orogenic belts, including the Qinling-Dabie orogen (Hacker et al., 1998; Faure et al., 1999), the Longmenshan belt (Yan et al., 2011), and the Indosinian orogen (Lepvrier et al., 2004). A Triassic deformation has also been recorded to the east of the study region in the Cathaysia block (Fig. 1), as documented by a Late Triassic unconformity and syn-orogenic magmatism at ca. 250-225 Ma (BGMRJX, 1984; BGMRGX, 1985; BGMRHN, 1988; Faure et al., 1996). The NE-SW trending Xuefengshan Belt, located in the central part of the South China Block, represents an important intracontinental orogen within the Early Mesozoic tectonic framework of East Asia (Fig. 1). Along with the Jiuling Belt, the Xuefengshan Belt formed a tremendous intracontinental belt characterized by NE-SW to NNE-SSW trending folds and faults with an overall northwest vergence (Fig. 1; Chu et al., 2012a, 2015; Chu and Lin, 2014).

2.2. The Xuefengshan Belt

2.2.1. Stratigraphy

In the stratigraphy of the Xuefengshan Belt, the deepest layer is the Mesoproterozoic-Neoproterozoic series, which, from bottom to top, can be subdivided into the Lengjiaxi group (Mesoproterozoic-Early Neoproterozoic), the Banxi Group (Middle Neoproterozoic) and the Sinian Group (Late Neoproterozoic) (BGMRHN, 1988). The Lengjiaxi group, containing mica schist, quartzite, meta-sandstones, phyllites and slates, is unconformably overlain by the Banxi group that includes conglomerate, sandstone and siltstone (BGMRHN, 1988; Wang et al., 2012). The Sinian Group consists of tillite, sandstone, chert and limestone. Two layers of tillite in this group, the Jiangkou Formation and Nantuo Formation, are interpreted to be deposited during global glaciation events (Zhang et al., 2005). Marine sedimentation continued until Early Triassic, except a stratigraphic gap between Middle-Late Silurian and Early Devonian followed by Middle Devonian terrestrial conglomerates. The Triassic orogeny involved pre-Triassic strata and subsequently Upper Triassic-Cretaceous sedimentary rocks were deposited in numerous intracontinental basins (Wang et al., 2005; Li and Li, 2007; Shu et al., 2009; Chu et al., 2012a).

2.2.2. Deformation

Recent studies have examined the structural pattern and magmatism of the Xuefengshan Belt, and define the polyphase deformation and post-orogenic granitoids (Wang et al., 2005; Chu et al., 2012a, 2012b; 2012c). Two tectonic zones can be identified in the Xuefengshan Belt, the Western Zone and the Eastern Zone (Fig. 2). Another important tectonic feature is the Main Xuefengshan Thrust (MXT), which represents the cleavage front, and separates the metamorphosed rocks of

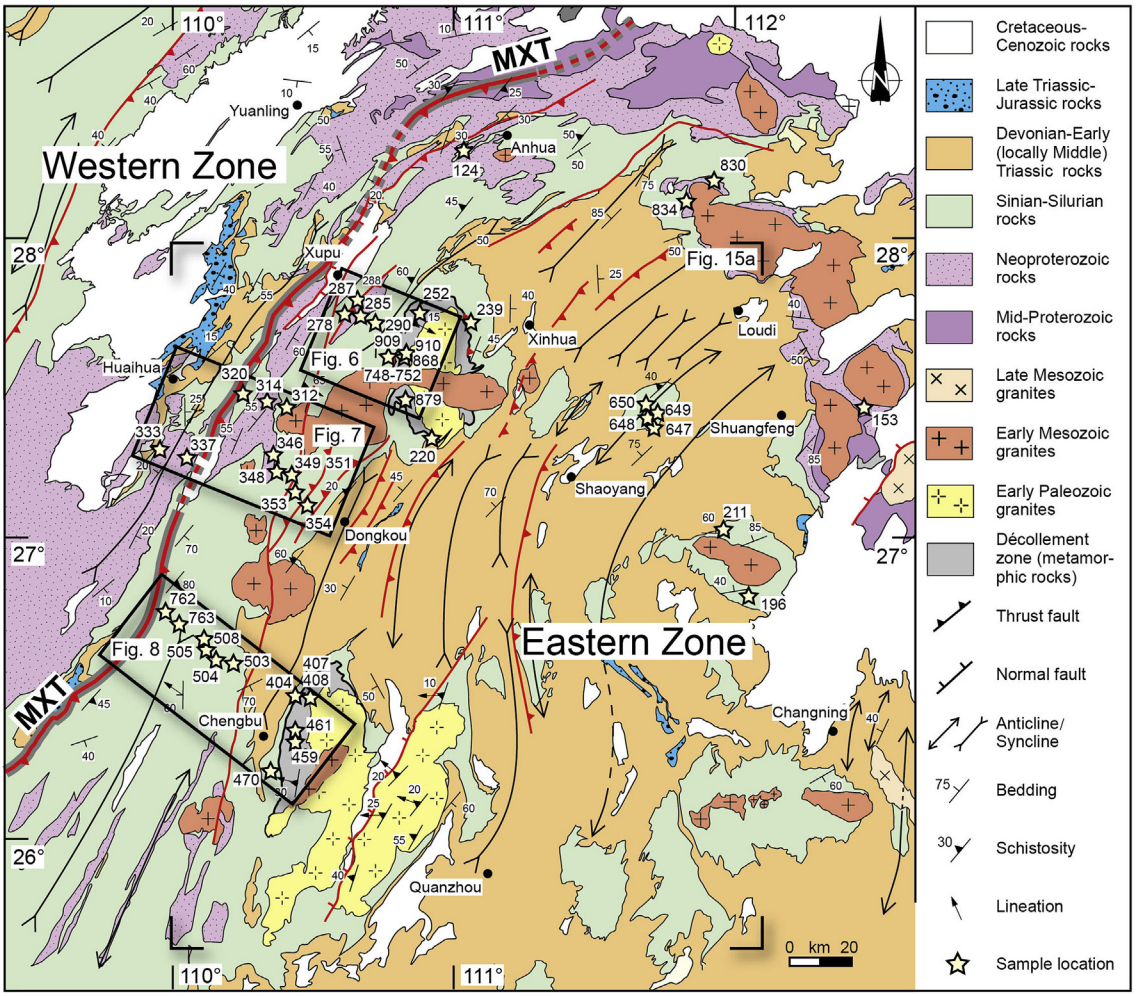

Fig. 2. Simplified geological map of the Xuefengshan Belt (Modified after Chu et al., 2012a). Sample locations for strain analysis are also indicated on the map. MXT: Main Xuefengshan Thrust. Separated by the MXT, the Xuefengshan Belt can be divided into the Western Zone and the Eastern Zone, which represent the higher structural and lower structural units, respectively.

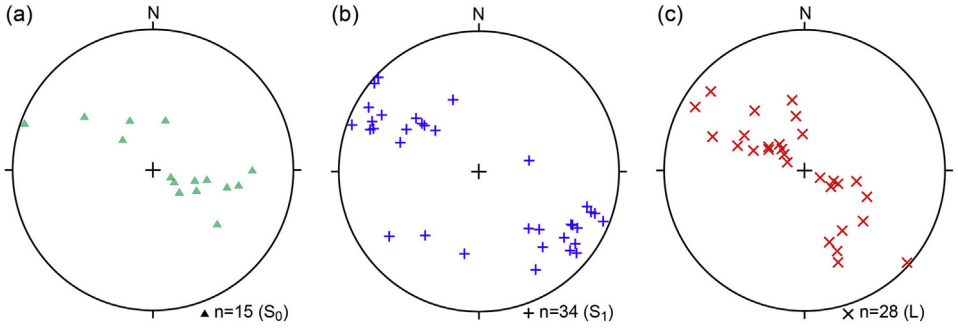

Fig. 3. Stereographic plots (Schmidt lower hemisphere projection) of structural elements from the Neoproterozoic conglomerates in the Xuefengshan Belt. (a): Poles to bedding. (b): Poles to schistosity. (c): Lineation.

the Eastern Zone and the non-metamorphosed rocks of the Western Zone (Chu et al., 2012a, Fig. 2). The Western Zone is characterized by km-scale box-fold structures with layer-slip and collapse folds in the limbs. In the Eastern Zone, NW verging folds coeval with a pervasive slaty cleavage and NW-SE trending lineation are the dominant structures. From west to east, the dip of the cleavage surface exhibits a fan-like pattern with back-folding and back-thrusting towards the southeast reshaping the NW-directed structures.

The architecture of the Eastern Zone results from polyphase deformation (Chu et al., 2012a) including: (1) D_1, characterized by a top-to-the-NW shearing, controls the bulk architecture of the Xuefengshan Belt, responsible for the crustal thickening of the deeper unit of the Eastern Zone; (2) D_2 corresponds to the back-folding and back-thrusting stage with preferential schistosities that dip to the NW. The S_1 cleavages were refolded by F_2 folds with relics preserved in some muddy layers; (3) D_3 is a NW-SE or W-E shortening event associated with upright folds with vertical axial plane cleavages. Both D_1 and D_2 structures were affected in the D_3 event. Based on previous work, three stages of deformation share similar orientation of lineation, and can be regarded as a continuous and cumulative process that occurred in the Triassic

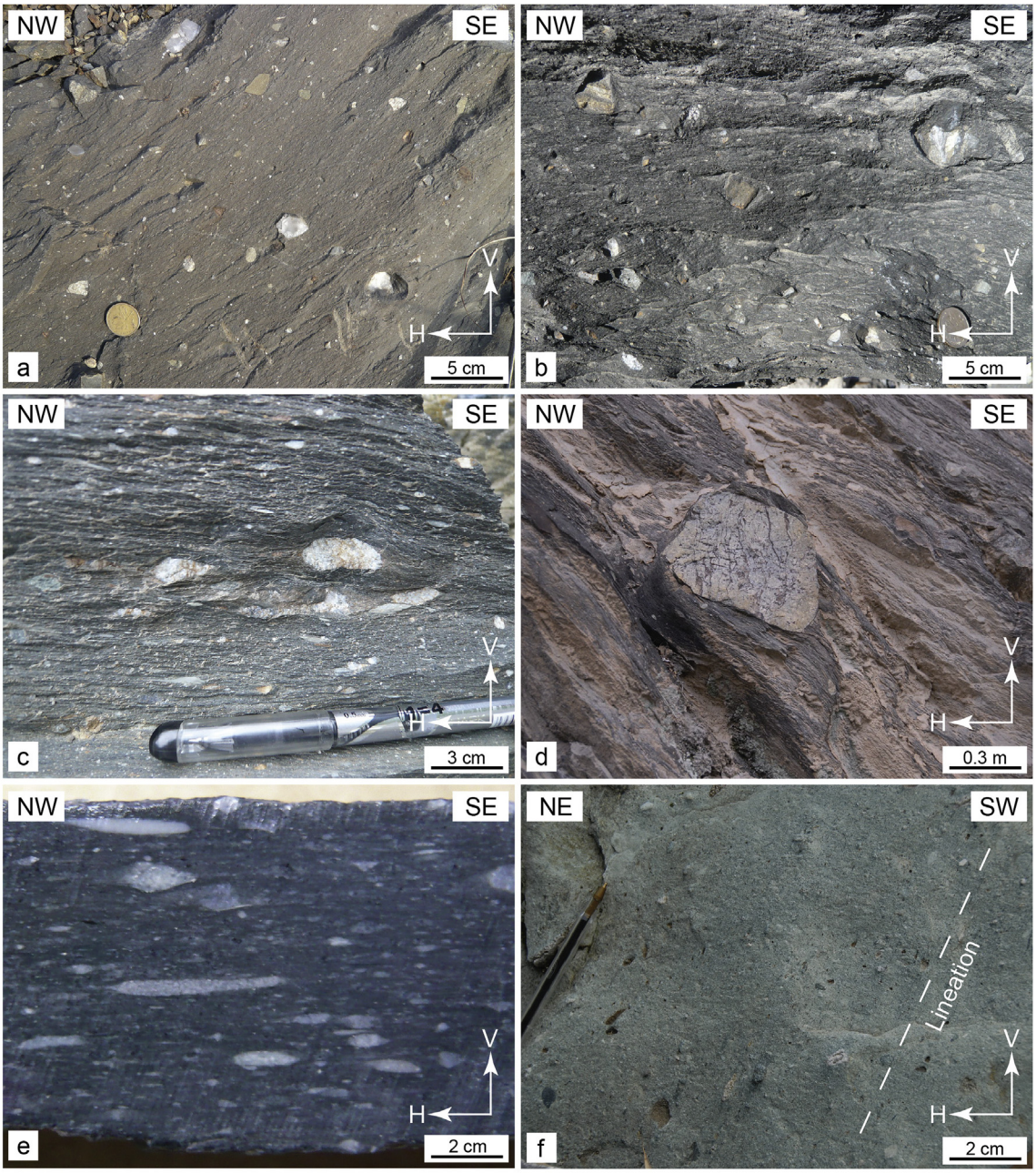

Fig. 4. Field photos of structures observed in the Neoproterozoic conglomerate displaying the variation of strain intensity and structures from undeformed to highly deformed rocks. V: Vertical. H. Horizontal. (a): Non-deformed tillite with randomly distributed pebbles in the pelitic matrix. (b): Slightly deformed conglomerate in which pebbles show no preferred orientation, but sparsely-spaced slaty cleavage is developed in the pelitic matrix. This difference of deformation style indicates a rheological contrast between pebbles and matrix that leads to distinct deformation patterns. (c): Well oriented pebbles parallel to the penetrative cleavage in highly deformed conglomerate. (d): Intensely sheared conglomerate with a sandstone boudin and high strained matrix. Note that strain shadow formed around the pebble indicates top-to-the NW shear sense. (e): Mylonitic conglomerate with strongly stretched pebbles and the direction of the long axis is parallel the foliation. (f): Lineation in highly deformed rocks comprised of elongated pebbles/clasts with a preferred direction.

intracontinental orogeny between 245 and 225 Ma (Chu et al., 2012a).

2.2.3. Ductile deformation in the décollement

A high strain zone, corresponding to the ductile décollement, accommodates at depth the deformation in the Neoproterozoic to Early Triassic sedimentary series (Chu et al., 2012b). This ductile synmetamorphic zone cropped out in the structural high uplifted by the emplacement of Late Triassic granites (Chu et al., 2012c), and subsequently was exposed to the surface by erosion. In this décollement, flat-lying foliation and NW-SE trending stretching and mineral lineation of micaschist and quartzite are exclusively developed with top-to-the NW shear sense, whereas evidence of later overprinting is lacking. Therefore, the three events recorded in the sedimentary cover are interpreted as a continuum of a single NW-SE contraction event in the décollement zone. A detailed study suggests that the deformation in the décollement mainly occurred during the Middle Triassic that is coeval with the timing of deformation in the sedimentary cover (Chu et al., 2012b).

3. Structures of the Neoproterozoic conglomerate

As the lower stratigraphic unit of the Xuefengshan Belt, the Neoproterozoic conglomerate, hereafter representing both the fluvial

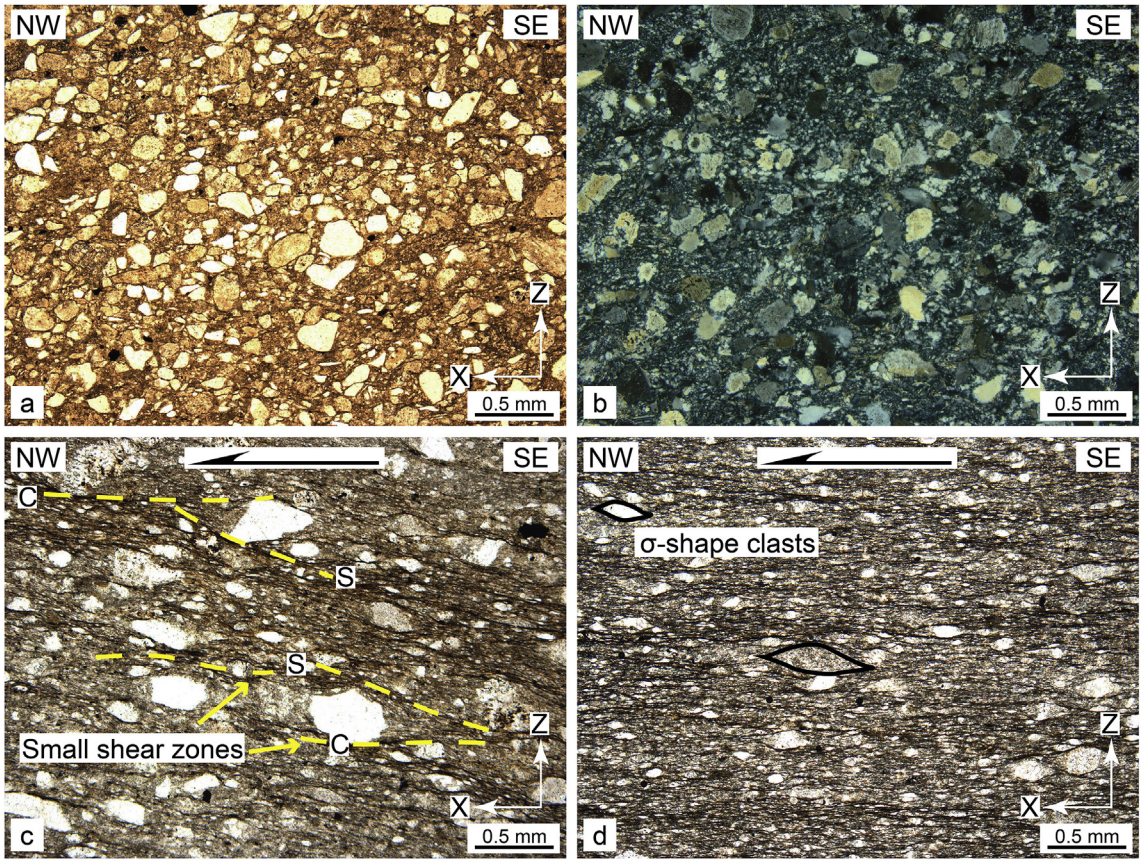

Fig. 5. Photomicrographs of Neoproterozoic conglomerates. (a): Non-deformed rock in which no orientation has been observed both in clasts and matrix. (b): Weakly deformed conglomerate with weak preferred orientation of clasts. (c): Well oriented clasts of quartz and feldspar in strongly deformed conglomerate. Note that some shear zones (dashed lines) truncating with each other may represent S-C fabrics and top-to-the NW shear sense is indicated. (d): Closely-spaced foliation and σ-shape clasts in mylonitic conglomerate, showing top-to-the NW shear sense.

conglomerates of the Banxi Group and tillites of the Jiangkou and Nantuo formations, generally experiences more intensive deformation and contains penetrative, closely-spaced schistosity. Structural elements, including bedding, schistosity, and lineation, show similar geometric and kinematic features (Fig. 3) as those in the whole belt (Chu et al., 2012a). In different tectonic levels, fabrics of conglomerate vary from undeformed to mylonitic. The upper tectonic level preserves primary sedimentary structures with random orientation of pebbles/clasts in non- or weakly deformed conglomerate (Figs. 4a and 5a). Under stronger deformation, strain concentration is illustrated by sparsely-spaced cleavage in the pelitic matrix, but pebbles still remain apparently undeformed and unrotated as rigid parts in conglomerate (Fig. 4b). Photomicrographs also show orientated clasts (Fig. 5b) and small shear zones in between large clasts as a result of strain localization (Fig. 5c). High-strain conglomerate, when approaching the décollement, is strongly sheared with penetrative schistosity and elongated pebbles (Fig. 4c–e), and contains shearing structures including strain shadows or σ-shape clasts (Fig. 5d). On the foliation plane, small pebbles are linearly aligned to form a stretching lineation parallel to regional contraction direction (Fig. 4f).

4. Methods for strain estimation

We firstly collected 48 oriented samples of (meta-) conglomerate and (meta-) sandstone in the field for strain analysis. For each sample location, we observed the whole outcrop and then chose a pebble-free part to collect the sample. Eighteen samples were analyzed from the Banxi Group, and thirty samples were analyzed from the Sinian Group including five from the Nantuo Formation and twenty-five from the Jiangkou Formation (Table 1). In the study area, despite the polyphase deformation, consistent kinematics during the Triassic orogeny had been observed in the Xuefengshan Belt. Hence, we assumed these phases as one continuous deformation, and thus 2D strain analysis in XZ and YZ planes can reflect the strain ellipsoid in selected samples. In order to reduce the bias of strain caused by quantification on different scales between conglomerate and sandstone samples, we measured clasts in thin sections, and then obtained strain ratios for all samples. In this study, as the portion of pebbles is much lower than the matrix, we thus assume that strain is concentrated in conglomerate matrix at outcrop scale. On the other hand, photomicrographs of conglomerate matrix and sandstone show similar composition and structure that allow us to compare the strain results acquired in both rock types. Two oriented thin sections were cut from rock samples in the XZ and YZ planes of finite strain (XZ: perpendicular to the foliation and parallel to the lineation; YZ: parallel to the foliation and perpendicular to the lineation). In case that lineation is not well-developed, the XZ plane is perpendicular to axial planes of crenulation or folds. If crenulation or folds are not developed in the sampling location, the XZ plane was approximated by cutting an oriented thin section along the regional shortening direction (N120°).

In order to estimate finite strain, the Rf/φ method is adopted here to study the clasts in matrix of conglomerates or sandstones (Ramsay, 1967; Dunnet, 1969; Lisle, 1985). Under microscope, the meta-conglomerate/sandstone is grain supported with clasts average > 70% by volume, and thus suitable for Rf/φ method (Okudaira and Beppu, 2008; Long et al., 2011; Tull et al., 2012). To reduce any effect of compositional bias, we also cut at least 2 thin sections for every profile (XZ or YZ), and then selected the one with similar composition to outcrop for

Table 1
Sample information and calculated strain results for Neoproterozoic rocks of the Xuefengshan Belt.

Sample number	GPS		Map unit	Lithology	Bedding[a]	Foliation (XY)	Stretching lineation	X direction[b]	Mineralogy[c]	Crenulation or fold axis	Strain ratios								3D ellipsoid:
	Longitude	Latitude							Qz-Fs-Lt (%)		Rs-XZ	2σ	φ (XZ)	2σ	Rs-YZ	2σ	φ (YZ)	2σ	X:Y:Z
124	28°20.254'	111°06.304'	Jiangkou Formation	Sandstone	194, 30	10, 50	350, 48	-	70-25-5		1.14	0.13	-20	12	1.04	0.14	-27	11	1.14 : 1.04 : 1
153	27°28.205'	112°27.825'	Banxi Group-M[d]	Meta-sandstone		300, 66	300, 66	-	80-20-0		2.50	0.34	8	5	1.40	0.14	-13	10	2.50 : 1.40 : 1
220	27°23.361'	110°55.947'	Banxi Group-M	Meta-sandstone		155, 32	160, 31	-	75-20-5		2.92	0.28	-6	4	2.62	0.26	-6	4	2.92 : 2.62 : 1
239	27°44.775'	111°05.691'	Jiangkou Formation	Conglomerate		290, 77	(300, 77)[e]	210, 37	60-30-10		1.45	0.17	-16	8	1.36	0.23	7	9	1.45 : 1.36 : 1
252	27°45.636'	111°06.676'	Banxi Group-M	Quarzite		300, 5	120, 5	-	65-30-5		2.84	0.28	-1	4	2.44	0.27	-1	4	2.84 : 2.44 : 1
278	27°47.960'	110°36.976'	Nantuo Formation	Conglomerate		130, 49	148, 48	-	70-20-10		1.87	0.27	7	7	1.78	0.18	6	6	1.87 : 1.78 : 1
285	27°48.350'	110°36.669'	Nantuo Formation	Conglomerate		160, 45	161, 45	71, 1	60-30-10		1.58	0.18	4	9	1.54	0.17	-16	6	1.58 : 1.54 : 1
287	27°46.585'	110°37.133'	Banxi Group	Conglomerate		130, 42	158, 38	-	75-20-5		1.76	0.13	1	4	1.69	0.15	6	6	1.76 : 1.69 : 1
288	27°46.079'	110°37.450'	Banxi Group	Sandstone	128, 52	133, 35	[120, 34][f]	-	70-25-5	30	2.32	0.14	0	3	2.28	0.19	1	5	2.32 : 2.28 : 1
290	27°44.525'	110°39.575'	Jiangkou Formation	Conglomerate	135, 25	133, 88	135, 88	-	80-20-0	45	2.52	0.15	-1	4	2.08	0.19	-1	4	2.52 : 2.08 : 1
312	27°27.865'	110°22.809'	Nantuo Formation	Conglomerate		307, 75	308, 75	-	75-20-5		2.02	0.16	11	4	1.57	0.13	-13	7	2.02 : 1.57 : 1
314	27°28.457'	110°21.413'	Banxi Group	Sandstone		130, 87	[130, 87]	-	60-30-10	40	1.78	0.26	-2	6	1.78	0.20	-2	5	1.78 : 1.78 : 1
320	27°29.041'	110°15.615'	Jiangkou Formation	Conglomerate		120, 50	(120, 50)	-	80-20-0		1.57	0.09	5	4	1.32	0.08	7	5	1.57 : 1.32 : 1
333	27°22.554'	109°56.407'	Jiangkou Formation	Conglomerate	310, 20	299, 14	(300, 20)	30, 0	60-35-5		1.26	0.07	14	5	1.16	0.07	-12	6	1.26 : 1.16 : 1
337	27°19.748'	110°03.490'	Jiangkou Formation	Conglomerate	110, 87	295, 28	(120, 87)	210, 3	65-30-5		1.40	0.12	-19	7	1.08	0.09	-28	9	1.40 : 1.08 : 1
346	27°19.605'	110°22.946'	Banxi Group	Sandstone		300, 70	305, 70	215, 13	70-25-5	35	1.98	0.20	-2	5	1.78	0.22	1	7	1.98 : 1.78 : 1
348	27°18.378'	110°23.554'	Jiangkou Formation	Sandstone		292, 85	(300, 85)	-	75-25-0		1.45	0.20	21	9	1.31	0.12	2	6	1.45 : 1.31 : 1
349	27°17.162'	110°24.612'	Jiangkou Formation	Sandstone		112, 70	(120, 70)	30, 21	70-30-0		1.78	0.17	-4	6	1.58	0.15	-22	4	1.78 : 1.58 : 1
351	27°16.414'	110°26.523'	Nantuo Formation	Sandstone		319, 45	[300, 43]	30, 18	75-20-5	30	1.72	0.14	-7	6	1.38	0.16	-5	8	1.72 : 1.38 : 1
353	27°11.586'	110°24.851'	Jiangkou Formation	Sandstone		310, 80	295, 79	-	85-15-0		2.68	0.23	9	4	1.72	0.18	-25	6	2.68 : 1.72 : 1
354	27°11.766'	110°25.534'	Jiangkou Formation	Conglomerate		288, 70	(300, 70)	-	80-15-5		1.64	0.16	10	7	1.46	0.20	-14	8	1.64 : 1.46 : 1
404	26°29.241'	110°26.212'	Banxi Group	Sandstone	299, 14	299, 14	310, 14	-	75-20-5		1.51	0.18	9	6	1.44	0.18	2	9	1.51 : 1.44 : 1
407	26°29.554'	110°27.056'	Banxi Group-M	Quarzite	295, 28	295, 28	(300, 28)	-	65-30-5		2.48	0.13	3	2	1.45	0.17	-7	9	2.48 : 1.45 : 1
408	26°29.490'	110°27.598'	Banxi Group-M	Meta-sandstone		283, 45	310, 42	-	80-20-0	40	2.75	0.27	4	4	1.84	0.42	13	10	2.75 : 1.84 : 1
459	26°29.859'	110°28.904'	Banxi Group-M	Quartz-schist		291, 11	300, 11	-	70-25-5	20	2.28	0.25	2	5	1.66	0.16	1	4	2.28 : 1.66 : 1
461	26°25.217'	110°27.187'	Banxi Group-M	Quarzite		310, 50	290, 48	-	60-35-5		2.52	0.38	-2	4	1.69	0.17	2	5	2.52 : 1.69 : 1
470	26°14.664'	110°22.583'	Jiangkou Formation	Conglomerate	280, 32	280, 32	290, 31	-	80-20-0		1.58	0.14	6	7	1.37	0.16	19	8	1.58 : 1.37 : 1
503	26°37.034'	110°08.170'	Nantuo Formation	Conglomerate	284, 25	284, 25	(300, 24)	210, 7	75-25-0		1.33	0.13	-35	10	1.21	0.16	-58	12	1.33 : 1.21 : 1

(*continued on next page*)

Table 1 (*continued*)

Sample number	GPS		Map unit	Lithology	Bedding[a]	Foliation (XY)	Stretching lineation	X direction[b]	Mineralogy[c]	Crenulation or fold axis	Strain ratios								3D ellipsoid:
	Longitude	Latitude							Qz-Fs-Lt (%)		Rs-XZ	2σ	φ (XZ)	2σ	Rs-YZ	2σ	φ (YZ)	2σ	X:Y:Z
504	26°37.532'	110°07.563'	Jiangkou Formation	Sandstone	270, 60	270, 60	291, 58	-	65-30-5		1.93	0.31	-13	6	1.52	0.17	1	5	1.93 : 1.52 : 1
505	26°39.383'	110°06.650'	Jiangkou Formation	Sandstone	280, 52	280, 52	320, 44	-	60-30-10		2.93	0.21	-16	7	1.75	0.19	-2	4	2.93 : 1.75 : 1
508	26°42.889'	110°03.917'	Jiangkou Formation	Sandstone		320, 60	(300, 58)	-	80-15-5		1.54	0.19	10	8	1.36	0.23	10	9	1.54 : 1.36 : 1
647	27°26.962'	111°44.444'	Jiangkou Formation	Conglomerate		311, 75	357, 69	267, 70	60-30-10		2.04	0.21	6	4	1.94	0.22	4	6	2.04 : 1.94 : 1
648	27°27.650'	111°44.111'	Jiangkou Formation	Conglomerate		308, 66	351, 58	-	50-40-10		1.81	0.16	6	6	1.58	0.25	-10	8	1.81 : 1.58 : 1
649	27°28.158'	111°44.172'	Jiangkou Formation	Conglomerate		300, 65	303, 65	-	60-30-10		1.78	0.18	-1	4	1.42	0.15	2	7	1.78 : 1.42 : 1
650	27°29.128'	111°44.591'	Jiangkou Formation	Conglomerate		314, 50	300, 49	30, 16	80-15-5		1.33	0.21	-2	10	1.17	0.21	-24	12	1.33 : 1.17 : 1
748	27°39.156'	110°46.851'	Jiangkou Formation	Conglomerate		120, 80	115, 80	-	85-15-0		2.52	0.40	3	7	1.45	0.34	4	11	2.52 : 1.45 : 1
749	27°38.965'	110°46.980'	Jiangkou Formation	Conglomerate		120, 69	112, 69	-	70-25-5		1.60	0.38	3	9	1.18	0.15	6	10	1.60 : 1.18 : 1
750	27°38.694'	110°47.127'	Jiangkou Formation	Conglomerate		110, 72	110, 72	-	80-15-5		1.93	0.27	6	6	1.38	0.20	6	9	1.93 : 1.38 : 1
752	27°38.431'	110°47.706'	Jiangkou Formation	Conglomerate		330, 70	316, 69	-	80-20-0		2.70	0.20	0	5	1.81	0.15	2	3	2.70 : 1.81 : 1
762	26°49.371'	109°59.486'	Jiangkou Formation	Conglomerate		115, 73	122, 72	-	75-25-0		2.41	0.23	8	3	1.91	0.13	8	3	2.41 : 1.91 : 1
763	26°48.365'	110°00.387'	Jiangkou Formation	Conglomerate		110, 50	113, 50	-	70-20-10		3.21	0.33	7	2	2.12	0.23	2	3	3.21 : 2.12 : 1
784	26°32.082'	109°44.704'	Nantuo Formation	Conglomerate		130, 44	131, 44	-	60-25-15		1.26	0.11	-6	6	1.16	0.15	-6	11	1.26 : 1.16 : 1
830	28°11.487'	111°58.211'	Banxi Group-M	Quarzite		40, 50	132, 2	-	90-10-0		2.53	0.32	3	4	1.90	0.20	1	7	2.53 : 1.90 : 1
834	28°08.956'	111°52.927'	Banxi Group-M	Quarzite		54, 68	102, 59	-	60-35-5		2.47	0.32	7	4	1.93	0.20	-13	5	2.47 : 1.93 : 1
868	27°46.540'	110°52.693'	Banxi Group-M	Quarzite		290, 74	313, 72	-	70-25-5	45	1.96	0.37	-81	19	1.66	0.25	-61	12	1.96 : 1.66 : 1
879	27°29.794'	110°51.792'	Banxi Group-M	Quarzite		258, 30	[300, 23]	-	75-20-5	30	2.17	0.27	-15	5	1.69	0.22	-17	8	2.17 : 1.69 : 1
909	27°35.942'	110°50.240'	Banxi Group-M	Quarzite		290, 40	330, 33	-	80-20-0	60	2.71	0.29	-9	4	2.08	0.23	10	6	2.71 : 2.08 : 1
910	27°36.201'	110°49.922'	Banxi Group-M	Quarzite		290, 40	320, 36	-	85-15-0		2.60	0.31	-3	5	2.36	0.35	1	4	2.60 : 2.36 : 1

[a] The occurrence of bedding, foliation and stretching lineation is shown as **azimuth, dip angle**.
[b] When X direction is differernt from the lineation after strain analysis, the number is indicated.
[c] We use clast ratios to represent the mineralogy of selected samples. Qz: Quartz. Fs: Feldspar. Lf: Lithic fragments.
[d] This sample belongs to the Banxi Group that has been metamorphsed.
[e] When the lineation and crenulation/fold are absent, we choose N300° (NW-SE) as the lineation direction and mark them in round brackets (Data from Chu et al., 2012a).
[f] When the lineation is absent, we choose the direction perpendicular to the crenulation/ fold axis as the lineation direction and mark them in square brackets.

strain analysis. In photo micrographic scale, clasts in matrix, including single quartz/feldspar grains or lithic fragments, were analyzed by the Rf/φ method to measure the strain accumulated within matrix as a better estimate of the bulk strain. In this method, Rf represents aspect ratios of the final shapes of clasts, and φ is the angle between the long axis of clasts in the deformed rock and the reference line. The reference line is defined here as cleavage in non-metamorphic rocks or foliation in metamorphic rocks. The angle φ ranges from −90° to 90°, with NW-dipping in the XZ plane and NE-dipping in the YZ plane being positive, respectively.

All thin sections were photographed under a microscope, and these images were processed by using the software "**NIH ImageJ**" (Free download at https://imagej.nih.gov/ij/) to obtain the long/short axis ratios and orientations of quartz/plagioclase or lithic clasts in both XZ and YZ planes. This software can automatically generate best-fit ellipses of clasts and produce measurement-orientation of both long and short axes (Detailed procedures see Bjørnerud and Boyer, 1996; Treagus and Treagus, 2002). At least fifty clasts for each sample were analyzed in this software and the exported results were entered into the "Excel Spreadsheet" of Chew (2003) to calculate parameters of these samples, including (1) the harmonic mean R_f value of the sample, (2) the mean value of φ data, and (3) the value of R_s (Table 1). Uncertainty of data was generated by adopting the method described by Robin and Torrance (1987) for 2σ errors of Rs and φ data.

5. Strain analysis results

An overall of 48 samples, from Banxi Group, Jiangkou Formation and Nantuo Formation, have been analyzed to obtain aspect ratios and orientations of quartz/feldspar clasts. Among these samples, the clasts that were calculated include mostly single grains (quartz 60–80% and feldspar 15%–35%), and minor aggregates or lithic fragments (< 10%) with both quartz and plagioclase (Table 1). In this study, we separate the samples of the Banxi Group into two subgroups: (1) Banxi Group-M, which has been metamorphosed under lower greenschist facies, and (2) Banxi Group, free of metamorphism. Strain ellipses in the XZ plane have ratios (R_{XZ}) from 1.1 to 3.2, and in the YZ plane have ratios (R_{YZ}) from 1.0 to 2.7 (Table 1). To better understand the strain variation intimately tied to the thrust tectonics, three orogen-perpendicular sections are chosen to evaluate in detail the deformation mode and variation in the belt (Fig. 2).

5.1. North Section

Thirteen samples were collected in the east of the Main Xuefengshan Thrust, i.e. in the Eastern Zone (Fig. 6a). Several major thrusts expose lower structural units, and the final exhumation of the décollement is likely linked to the emplacement of Triassic plutons (Fig. 6b). All the sedimentary sequences have been intensely folded, resulting to penetrative cleavage in less deformed rocks, and foliation in strongly deformed rocks of the décollement, respectively. As part of décollement, Paleozoic granites are involved in the ductile shearing, whereas Early Mesozoic post-orogenic granites remain undeformed and crosscut previous structures.

In this section, of the twelve analyzed samples, ten have the longest R_s parallel to mineral stretching lineation in NW-SE, and two have the longest R_s in NE-SW (Fig. 6a). R_{XZ} and R_{YZ} ratios range from 1.5 to 2.9 and from 1.1 to 2.5, respectively (Table 1). Angles (φ) between bedding/schistosity and long axes of strain ellipses are mostly from −20° to 20°, and remain consistent with increasing R_{XZ} (Fig. 9a). The majority of samples plot in the flattening field of Flinn diagram, but two from Jiangkou Formation plot in the constriction field (Fig. 9d). The mean ellipsoid of all samples from this section is 2.2:1.8:1.0.

5.2. Middle Section

This region is characterized by a fold-and-thrust system upon the buried décollement at depth, resulting in duplexing and significant upper crustal shortening (Fig. 7a). Along the MXT, the deep-seated Neoproterozoic units of the Eastern Zone overthrust northwesterly onto the weakly deformed rocks of the Western Zone, and in the southeast back-thrust partly modified the NW-directed D_1 structures, both constituting fan-shape geometry in the core of the belt (Fig. 7b).

Strain results show that five samples have the longest Rs parallel to mineral stretching lineation in NW-SE, whereas five have the longest Rs in NE-SW, and one gives equal Rs values in both directions (Fig. 7a). Except sample 353, most samples yield low strain, with bulk strain ratios on the XZ planes ranging from 1.0 to 2.0, and those on the YZ planes ranging from 1.2 to 2.0. The majority of φ values are relatively low between −30° and 30°, and decrease with increasing R_{XZ} (Fig. 9b). On the Flinn diagram, all of the 11 samples plot in the flattening field (Fig. 9e). The mean ellipsoid of all samples of this section is 1.7:1.6:1.0.

5.3. South section

Similar to the North Section, the décollement zone crops out in the vicinity of Triassic plutons that assisted its final uplifting, and consists of greenschist facies metamorphic rocks including micaschist and quartzite (Fig. 8a). D_2 back-thrusting and back-folding dominates to the southeast of the MXT (Fig. 8b), but kinematic indicators preserved in deformed conglomerate show exclusively top-to-the NW shear sense formed in the D_1 stage (Chu et al., 2012a). Despite very low grade metamorphism, sedimentary bedding in Sinian conglomerates is almost replaced by closely spaced cleavages, along which pebbles and clasts are sheared and oriented.

In 12 out of the 13 samples, the X direction is parallel to stretching lineation (NW-SE), and only one has the longest R_S in NE-SW direction (Fig. 8a). R_{XZ} ratios demonstrate a relatively large range from 1.2 to 3.2, and R_{YZ} ratios range from 1.1 to 2.2, suggesting higher deformation intensity along the lineation (Table 1). Except samples 408 and 503, φ values of all samples are less than 20° (Fig. 9c). Comparatively, most samples plot in the flattening field of Flinn diagram similar to the results from the North and Middle Sections (Fig. 9f). The mean ellipsoid of all samples of this section is 2.1:1.6:1.0.

6. Discussion

6.1. Summary of strain analyses

Our new strain results illustrate general kinematic patterns of strain variation in the Xuefengshan Belt. The majority of data exhibit R_{XZ} of 1.0–3.2 and φ values < 30° in R_{XZ}-φ diagram, with generally consistent strain values among all the samples, but an overall correlation between increasing ratio and decreasing angle can also be observed (Fig. 10). From low strain (R_{XZ} = 1.0–2.0) to high strain (R_{XZ} = 2.0–3.2) rocks, shallowly dipping schistosity (φ < 30°) reflects a principal effect by thrust-normal flattening with a subordinate component of thrust-parallel shearing. It is also noteworthy that φ values of high strain rocks are relatively lower (φ < 20°) and thus suggests that effect of thrust-normal flattening is rising. In general, almost all samples are plotted in the flattening field (Fig. 11), indicating that thrust-normal flattening mechanism dominates the strain propagation throughout the entire fold-and-thrust belt; however, a difference exists among the three sections. In the Middle and South Sections, many of the data plot near the plane-strain line, suggesting that a higher thrust-parallel shearing component on rock deformation. On the contrast, the North Section includes mostly thrust-normal flattening with some minor thrust-parallel shearing (Fig. 9a).

The strain data from the Xuefengshan Belt indicate NW-SE shortening with mostly orogen-perpendicular elongation of strain ellipsoid

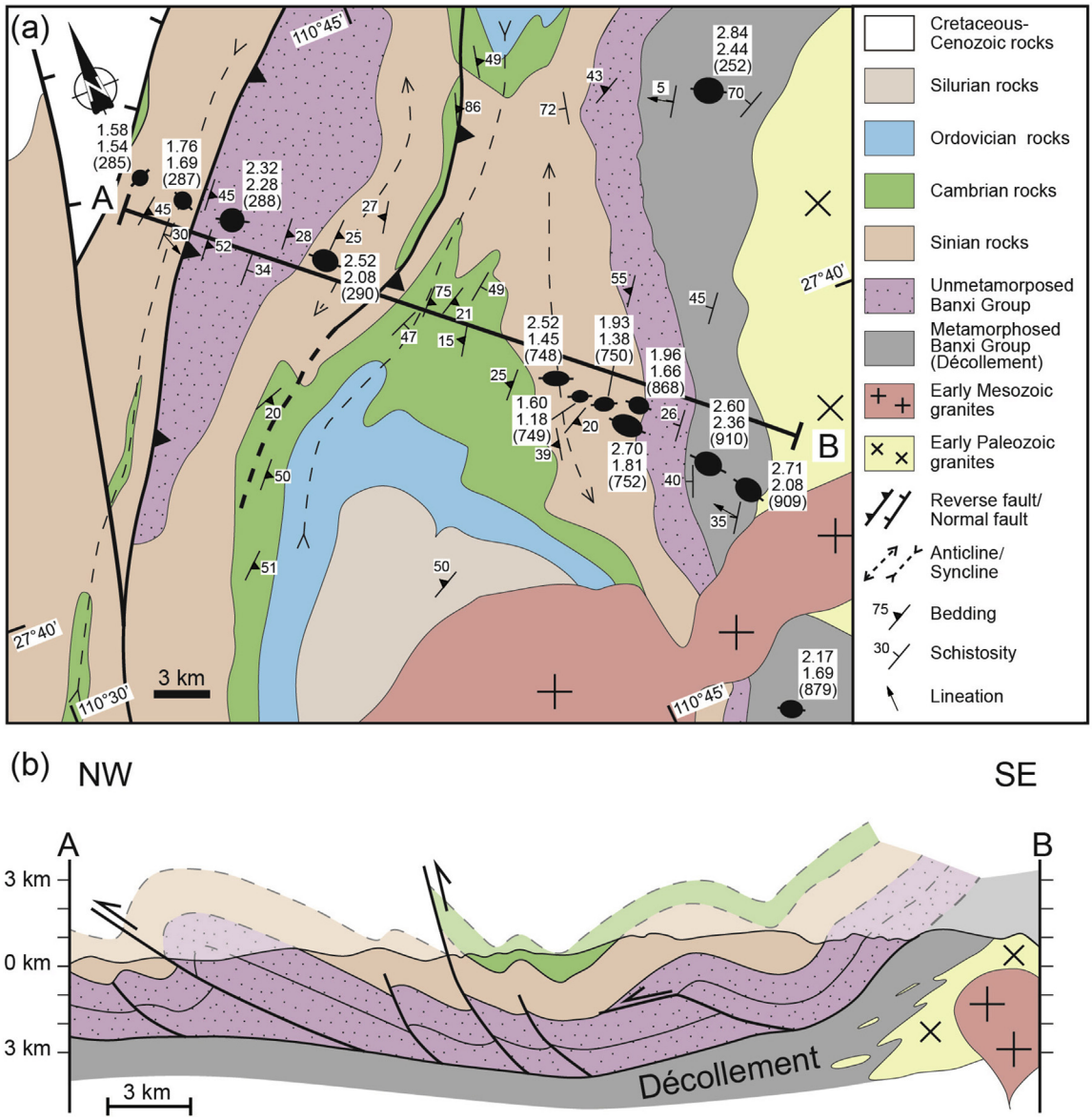

Fig. 6. (a): Regional geological map of the North Section (Modified after BGMRHN, 1988). Location is marked on Fig. 2. Strain ratios on XZ and YZ planes, and sample numbers are labelled on the map. (b): Cross-section of the study region that provides a detailed geometry and thrust structures. The regional décollement is located beneath the sedimentary cover but the eastern part has been uplifted during tectonic imbrication and Triassic granite emplacement.

(Figs. 6–8). However, it is notable that some samples that yield low strain ratios recorded orthogonal stretching parallel to regional fold axes and perpendicular to mesoscopic lineations. This phenomenon can result from different tectonic regimes, including shortening in external, unmetamorphic thrust sheets (Mitra, 1994; Long et al., 2011; Tull et al., 2012), transpressional deformation in orogenic belts (Hartz and Andresen, 1997), or extensional structures during sustained contraction (Avigad et al., 2001; Charles et al., 2009). In the Xuefengshan Belt, there is no evidence to suggest transpressional deformation but all structures are developed under NW-SE shortening. Meanwhile, orogen-perpendicular extension also lacks field evidence both in the sedimentary cover and décollement (Yan et al., 2003; Chu et al., 2012a). Our data therefore support the model that low magnitude orogen-parallel stretching may develop firstly in the outer part of the Xuefengshan Belt, and strain ellipsoids are modified by subsequent shortening, but some initial feature is preserved due to the heterogeneity of deformation intensity.

In order to better quantify the relative contributions of pure shear and simple shear deformation, we also estimate mean kinematic vorticity numbers (W_m) of samples that are approximated to be deformed under steady-state, plane-strain deformation as a premise for further calculation and interpretation in this study (Means et al., 1980; Law et al., 2004; Long et al., 2011). W_m is defined as the non-linear ratio of pure shear ($W_m = 0$) and simple shear ($W_m = 1$) component of deformation (Means et al., 1980; Means, 1994), whereas pure and simple shear components make equal contributions at $W_m = 0.71$ (Law et al., 2004). W_m values are estimated by plotting our data on the log R_{XZ} vs. φ diagram (Fig. 12). Most high strain samples ($R_{XZ} = 2.0–3.2$) have concentrated W_m values from 0 to 0.7, and over two thirds of analyses are lower than 0.4. For low strain analyses ($R_s = 1.0–2.0$), W_m values range from 0.0 to 0.8, with the majority yielding values < 0.4. Based on the overall W_m analyses, both high and low strain rocks show comparable results with $W_m < 0.7$, as suggestive of a larger component of pure shear deformation rather than simple shear deformation (Law et al., 2004). All samples have α values plotted in the zones of $\alpha > 1.0$, and most of them are higher than 1.25 (Fig. 12). Consistent with our Flinn diagram (Fig. 11), this parameter suggests that the deformation includes thrust-parallel shearing and stretch in the direction

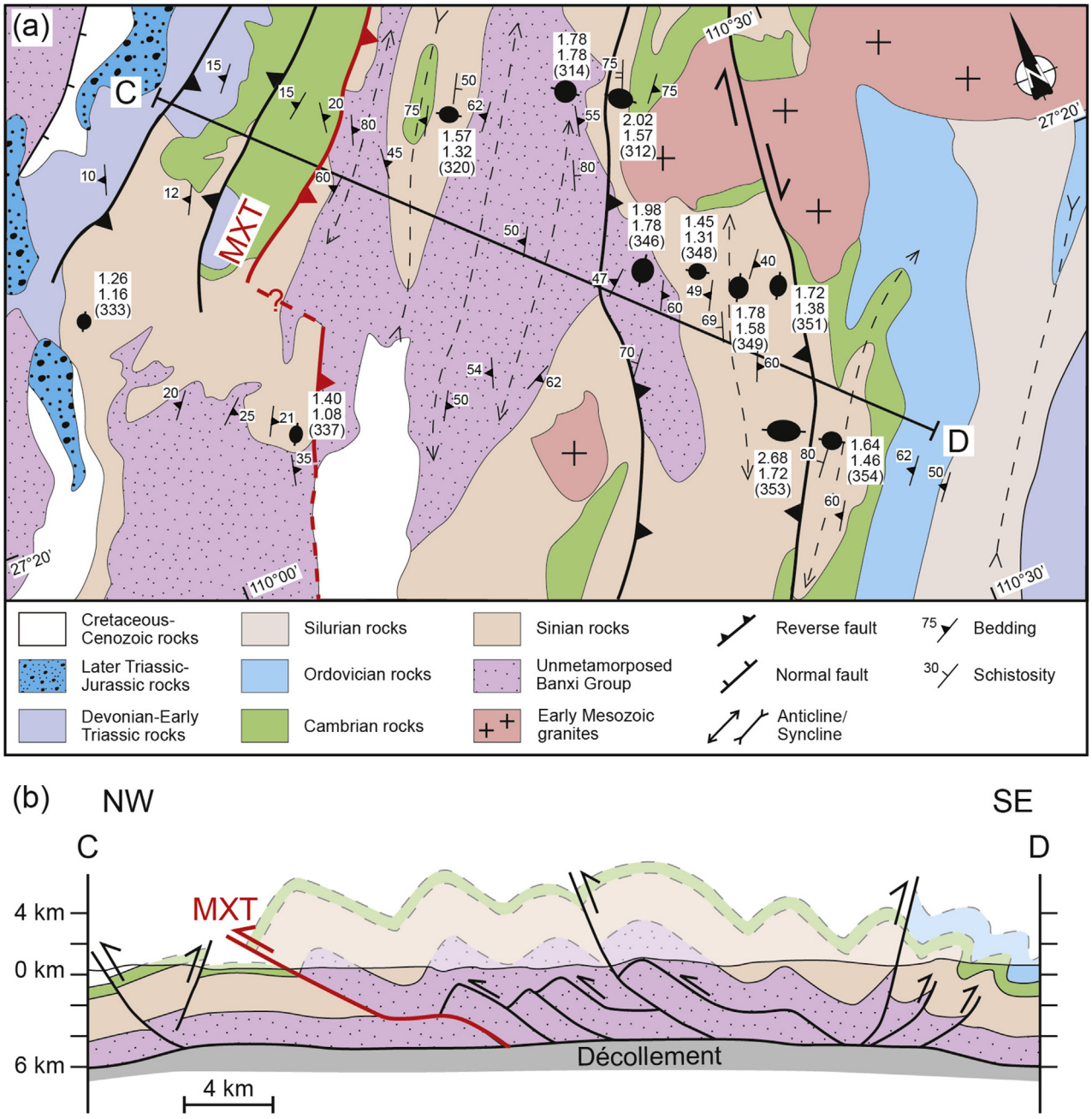

Fig. 7. (a): Regional geological map of the Middle Section (Modified after BGMRHN, 1988). See location on Fig. 2. Strain ratios on XZ and YZ planes, and sample numbers are indicated on the map. (b): Cross-section of the study region that provides a detailed geometry and kinematics. Note the deformation discrepancy on the western and eastern sides of the MXT. To the west, deformation is relatively weak, whereas intense thrusting and duplexing developed to the east. This cross-section is simplified by neglecting small scale folds and thrusts.

of thrust with a component of stretch that is perpendicular to thrusting direction.

Integrated with previous studies on microstructures on deformed rocks, strain pattern of the Xuefengshan Belt corroborates low temperature deformation (300–400 °C) with greenschist facies metamorphism (Chu et al., 2012b). Pure shear and thrust-normal flattening dominated deformation governed thrust-parallel schistosity formation and pebble reorientation in the D_1 stage. Low to intermediate strain ratios may result from diffuse deformation accumulated in the belt while high strain localized in the décollement implies significant strain partitioning, and this process will be further discussed in the next section.

6.2. Strain gradient in the Xuefengshan Belt

Ratios of strain ellipses (R_{XZ}) in the profile plane support a systematical variation dependent on structural positions (Fig. 13). As the uppermost analyzed unit in this study, the Nantuo Formation has relatively low R_{XZ} values of 1.2–2.0 and a median value at 1.46, consistent with field observation that suggests the lowest deformation grade of fabrics. At lower levels, strain increases in the Jiangkou Formation and Banxi Group with R_{XZ} values of 1.1–3.2 and 1.5–2.3 with median values at 1.71 and 1.78, respectively. At basal décollement levels, metamorphic Banxi Group has the highest strain ratios of 2.0–3.0 with a median value at 2.52 (Fig. 13). It is also noteworthy that several samples of the Jiangkou Formation yield high R_{XZ} values as the

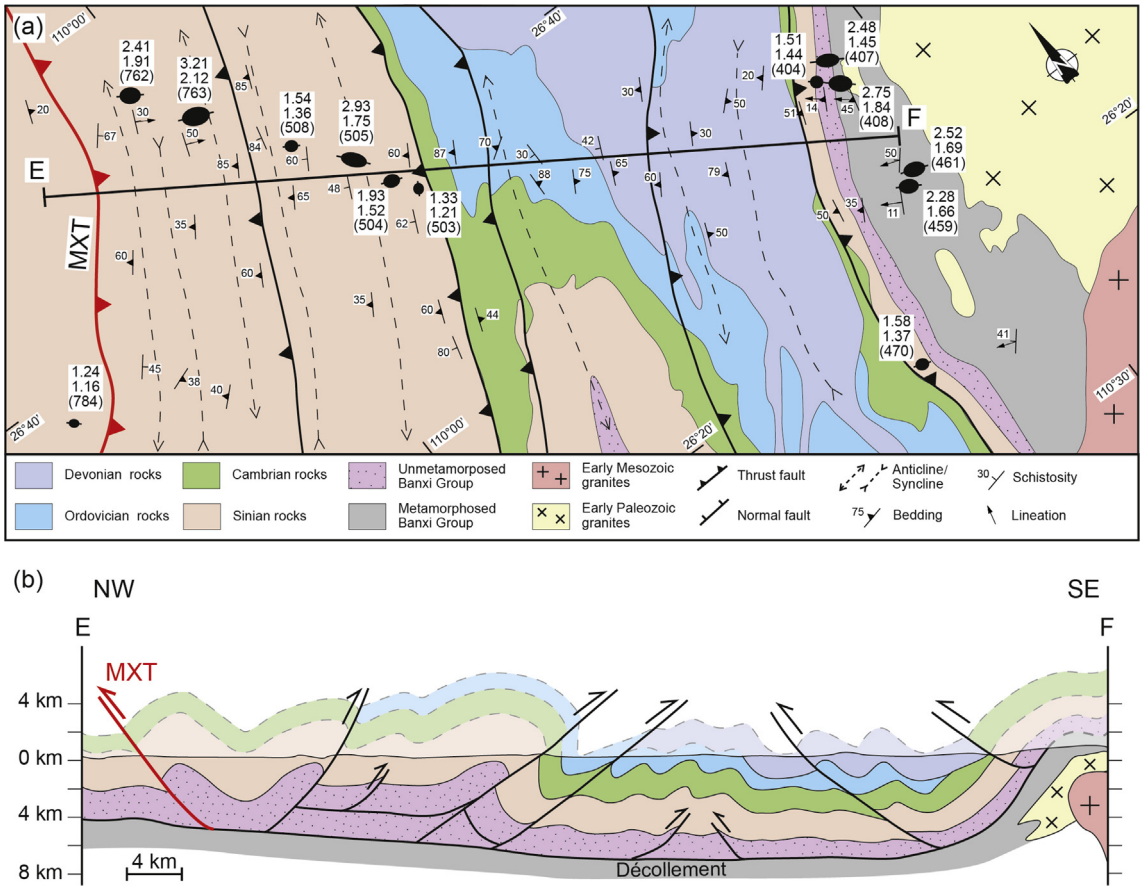

Fig. 8. (a): Regional geological map of the South Section (Modified after BGMRHN, 1988). See location on Fig. 2. Strain ratios on XZ and YZ planes, and sample numbers are indicated on the map. (b): Cross-section of the study region showing a detailed geometry and kinematics. Top-to-the SE shearing is more developed in this region. The exhumed décollement zone yields high strain ratios.

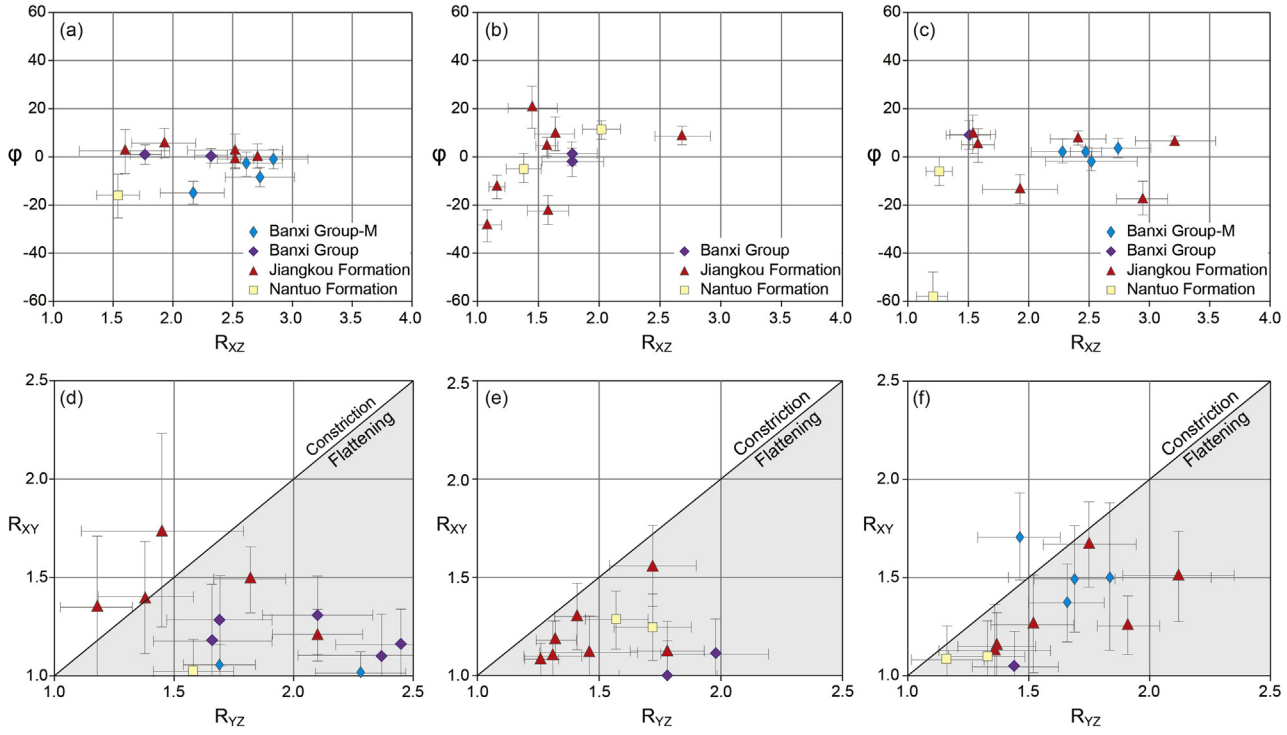

Fig. 9. Rxz-φ diagrams of the North (a), Middle (b) and South (c) Sections. Middle section yields lower strain ratios and higher angles than the rest two sections. Strain results are also plotted in Flinn diagrams for the North (d), Middle (e) and South (f) sections.

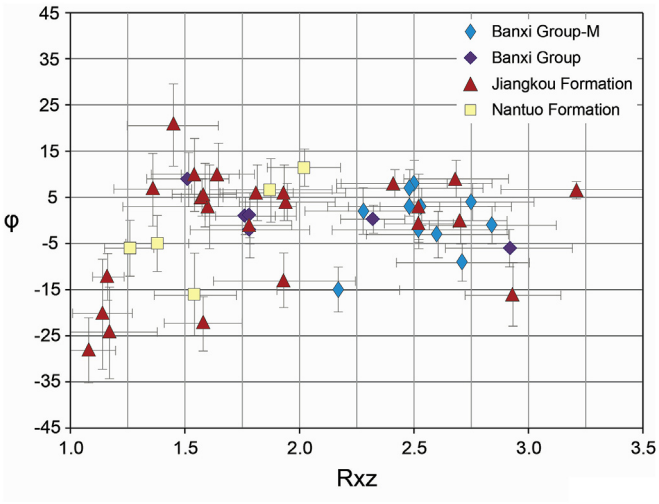

Fig. 10. Rxz-φ diagram for all the samples analyzed in this study.

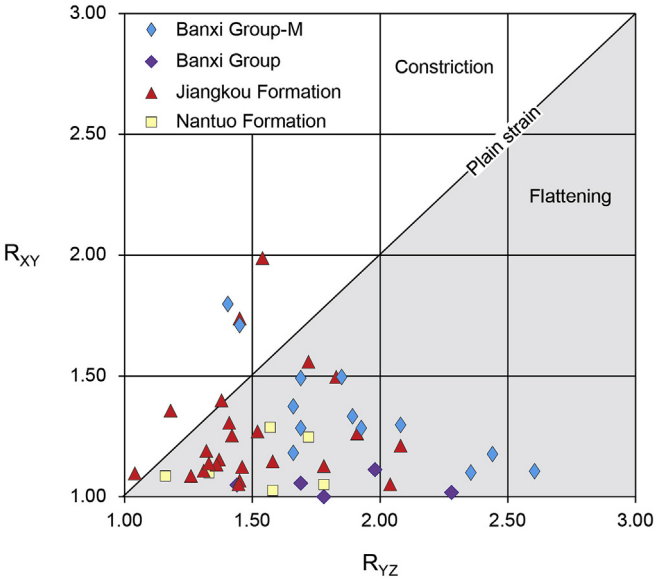

Fig. 11. Flinn diagram of all the samples analyzed in this study. Note that almost all samples are plotted in the flattening field.

metamorphic Banxi Group, indicating involvement in the high strain décollement zone. As a whole, bulk strain of analyzed samples gradually intensifies from the upper unit (Nantuo and Jiangkou Formations) to the lower unit (metamorphic Banxi Group), consistent with the trend of metamorphic grade and transition from brittle to ductile deformation (Chu et al., 2012b). Approaching to the décollement, strongly deformed samples from the Jiangkou Formation and metamorphic Banxi Group yield R_{XZ} strain ratios > 2.6, much higher than those of upper unit (R_{XZ} = 1.5–1.7) (Fig. 13). Strain patterns also suggest increasing thrust-normal flattening and decreasing thrust-parallel shearing. Notably, an underestimation of strain ratios in the rocks from the décollement zone may also exist in ductile conditions, because intracrystalline deformation of quartz grains accommodate part of external strain, and thus cannot be included by our strain calculation.

In terms of structural evolution, thrust-parallel schistosity observed in Neoproterozoic rocks probably formed during the D_1 stage, as testified by thrust-normal flattening at lower levels, and upwardly increasing component of thrust-parallel shearing, indicating an accumulative effect by D_2 back-folding and D_3 upright folding that only influenced the high levels. Based on the overall history of ductile

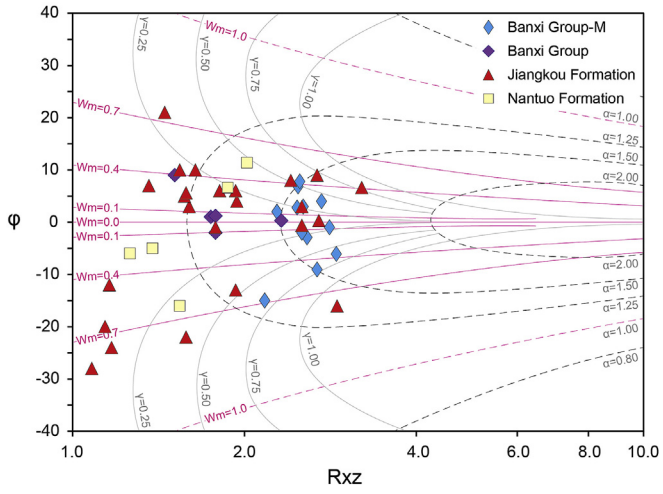

Fig. 12. Plots of Rxz vs. φ for all samples in the Xuefengshan Belt. Data are split out by stratigraphic formations. Contours of constant thrust-parallel shear strain (γ), ratio of thrust-parallel stretch to thrust-perpendicular stretch (α), and mean kinematic vorticity (W_m) are drawn from Yonkee (2005). Most samples have W_m < 0.7 that means a pure shear dominated deformation pattern.

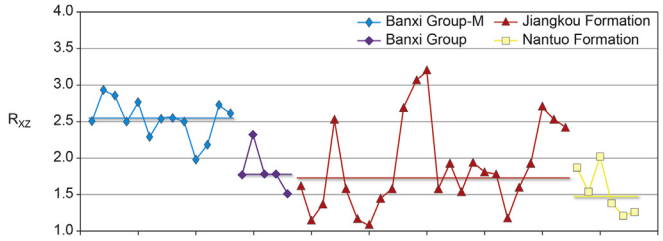

Fig. 13. Comparisons of strain ratios in R_{xz} planes for all analyzed samples. The Metamorphic Banxi Group has the highest values, while the Nantuo Formation yields the lowest value, and the Banxi Group and Jiangkou Formation have intermediate values. Lines in the middle of each group of samples are median values of Rxz ratios of the four groups, respectively.

deformation recorded in the Xuefengshan Belt (Chu et al., 2012a, 2012b), D_2 and D_3 may also played an important role in strain accumulation within the décollement zone decoupling the sedimentary cover and the basement as the only high-strain partitioning layer during polyphase deformation.

Our results of strain pattern recorded at low metamorphic grade in the Xuefengshan Belt show similarities with other fold-and-thrust belts. In the Moine Thrust Zone, less deformed quartzite has moderate strain ratios (R = 1.5–2) under thrust-parallel shearing, while mylonite yields extremely high strain (R = ~16), suggesting a similar pattern with strain concentration and thrust-normal thinning in localized high-strain zone (McLeish, 1971; Coward and Kim, 1981). The Willard thrust sheet of the Sevier fold-thrust belt displays an analogous model of deformation: the basal levels are characterized by high strain (R > 3.0) and thrust-subparallel foliation, and register a thrust-normal flattening dominated pattern; strain gradually decrease at higher tectonic levels with an increase of thrust-parallel shearing component, also implying a simple shear prevailing mechanism (Yonkee, 2005; Yonkee et al., 2013). Long et al. (2011) studied the foreland thrust belt of eastern Himalaya and documented that low temperature deformation under moderate layer-normal flattening strain (R = 1.8–2.0) controlled the formation of thrust sheets due to duplexing and subsequent overriding. Comparably, flattening strain has also been obtained by strain analysis in metachert samples from the Ryoke metamorphic belt, SW Japan, and is interpreted to record the schistosity-forming deformation, whereas constriction strain reflects modification by late folding events (Okudaira and Beppu, 2008; Okudaira et al., 2009).

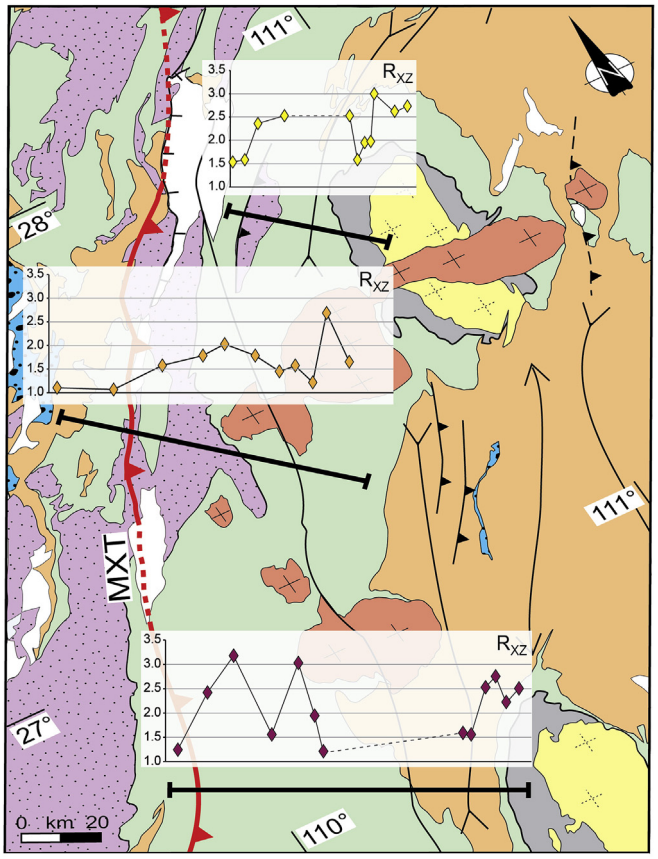

Fig. 14. Strain variation of three selected sections in the Xuefengshan Belt. An obvious decrease from the Eastern Zone to the Western Zone can be observed in the Middle and South Sections. It is noteworthy that strain ratios of the Middle section are significantly lower than those of the other two sections.

In most fold-and-thrust belts, thrust-normal flattening plays a significant role in strain accumulation of thrust sheets, and pure shear overrules under low temperature deformation (Yonkee, 2005; Long et al., 2011). Tectonic imbrication and loading lead to oblate strain fabrics with limited prolate strain, and this effect enhances at lower levels as temperature increases to induce crystal-plastic deformation. Hence, mid-crustal weaker horizons tend to concentrate shearing and then evolve into a basal thrust/décollement with the highest strain ratios, likely causing the strain partitioning process. Despite that incremental deformation may give rise to polyphase deformation that changes the orientation of strain ellipsoids in higher structural positions, the strain pattern in the lower units is still controlled by thrust-normal flattening with tectonic schistosity parallel to the basal décollement (Okudaira and Beppu, 2008; Yonkee, 2005; Long et al., 2011). Generally, lithology, presence of fluid, and temperature may lead to strain partitioning that generates gradient in deformed rocks, whereas strain pattern recorded in rocks from various structural positions reflects more information of the deformation history.

6.3. Along-strike strain variation and formation of the tectonic salient

Bounded by the MXT, kilometer-scale box folds predominate in the Western Zone involving shallow tectonic level units, whereas intensively deformed slate/schist of lower unit and sedimentary cover have NE-trending folds, schistosity and NW-SE lineation, characterizing the Eastern Zone (Qiu et al., 1998; Wang et al., 2005; Chu et al., 2012a). Most structures imply top-to-the NW brittle-ductile deformation, but top-to-the SE back-folding also dictates the geometrical mode of this belt, indicating a reverse transport during persistent shortening. Our strain data displays an orogen-perpendicular variation intimately associated with the geometry. To the west of the MXT, strain ratios (R_{XZ}) decrease significantly to 1.0–1.2 in the Western Zone from higher strain values ($R_{XZ} > 1.5$) in the Eastern Zone (Fig. 14), which argues for the juxtaposition of two tectonic units in different tectonic levels. Adjacent to the décollement in the east of the belt, intensified strain recorded in the deformed micaschist-quartzite corresponds well to the domal shape of exposed high-strain rocks.

Along strike, a distinctive variation with higher strain accumulated in the Northern and Southern Sections, where décollement zones are exhumed, exists in the Xuefengshan Belt, suggesting inhomogeneous deformation during the propagation of this belt. Most strain ratios in the Middle Section show low values ($R < 2.0$), while the other two sections include a large proportion of high values ($R > 2.0$). Such pattern is consistent with the field observation of deformation that rocks of the Middle Section experienced very low grade of metamorphism and limited tectonic uplifting (Fig. 14). Along-strike strain variation also coincides with the orogenic curvature of the Xuefengshan Belt, represented by curved anticlines/synclines and thrust systems. Spatially, this curvature is located between large Paleozoic batholiths, the Baimashan Batholith in the north and the Yuechengling Batholith in the south. Linear exposures of Early Paleozoic sedimentary rocks uplifted by Triassic tectonics also correspond well with the locations of these batholiths (Fig. 15a), as indicative of stress barriers during the propagation of the thrust belt. Previous studies have demonstrated that rheological contrasts induce diverse strain patterns in different rocks types, among which plutonic rocks are more rigid than clastic (Treagus and Treagus, 2002) or volcanoclastic rocks (Treagus and Treagus, 2002; Czeck et al., 2009). This result is in concert with geological observations upon the orogenic curvature in the Xuefengshan Belt. As recorded in the North and South Sections, strain was more accumulated to the west of these stiffer granitic batholiths, which resisted most of deformation but only suffered limited shearing at their peripheries. The Early Paleozoic strata to the east of batholiths were likewise uplifted by intensified compressional stress. On the contrary, an averaged, low strain pattern in the Middle Section and its eastern extension coincides with diffusive deformation and moderate uplifting, and folds and thrusts can migrate more to the west to form the arcuate shape (Fig. 15a).

Weil and Sussman (2004) subdivided curved thrust belts into three categories: (1) Primary arcuate belts that inherit their shapes from original geometry before initial deformation; (2) Progressive arcuate belts develop gradually by an incremental compression; (3) Oroclines that experience later deformation by bending their originally linear shape. According to our strain data and structural analysis, we can attribute the Xuefengshan Belt as a progressive arcuate belt for persistent advancing of deformation front and therefore illustrate its tectonic scenario during the Early Mesozoic (Fig. 15b–c). The initial compression formed firstly a linear belt with a top-to-the WNW shearing sense, corresponding to the D_1 stage that generated pervasive SE-dipping schistosity and kilometer to decimeter scale, asymmetrical folds above the décollement (Wang et al., 2005; Chu et al., 2012a, 2015). Accompanying the incremental deformation, the linear belt propagated toward the west, but encountered the Early Paleozoic batholiths that acted as rigid blocks. Consequently, strain was transferred to the west of the batholiths and resulted in high strain ratios in the North and South Sections. On the other hand, back-thrusting and folding related to the D_2 deformation led by batholith obstruction may be responsible for the tectonic uplifting of Early Paleozoic rocks in the east (Fig. 15c). Concurrently, the central part of the fold-and-thrust system grew westward to form the Dongkou salient but low paleo-relief was preserved by diffusive strain and limited uplifting. Such structural pattern reflects an interacting process between the thrust wedge and batholith barriers that created the curvature of the Xuefengshan Belt, which can be extracted from detailed strain analysis on the internal deformation patterns of fold-and-thrust belts.

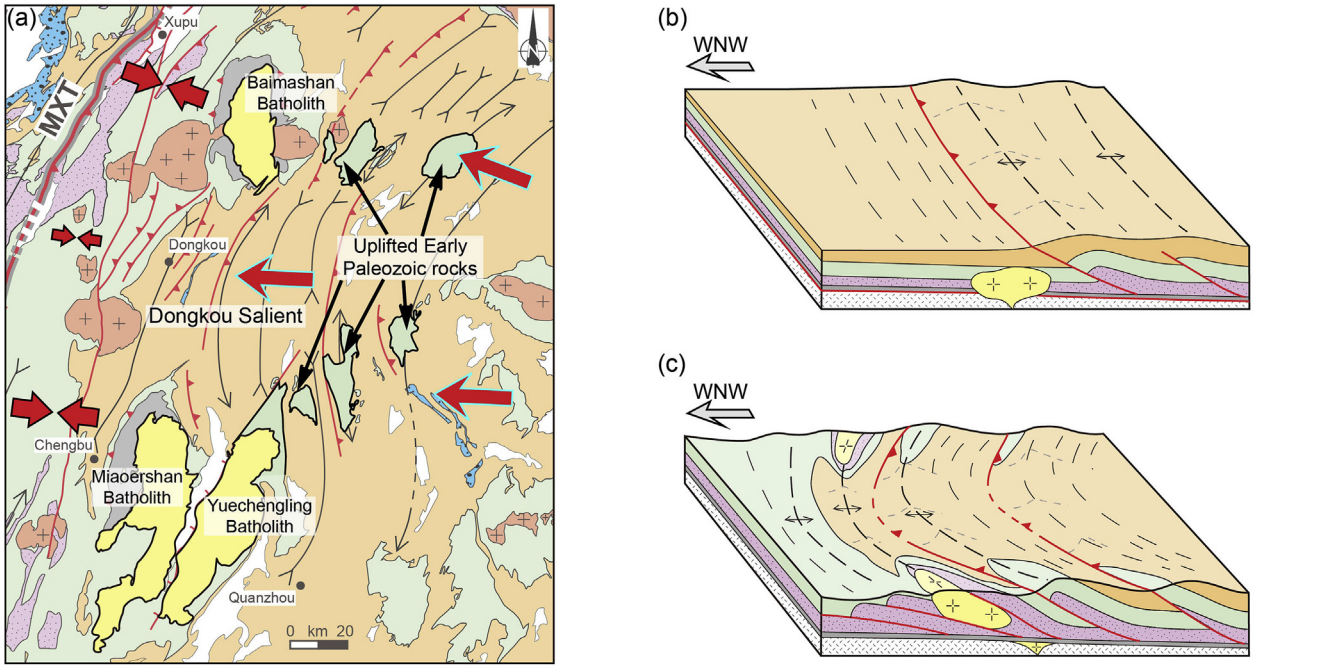

Fig. 15. (a): Detailed structural map shows the deformation pattern of the orogenic curvature. Paired red arrows represent the strain intensity as indicated by our results. Single arrows represent the direction of thrust propagation. Granitic batholiths and uplifted Early Paleozoic rocks are highlighted. A tentative tectonic model illustrating the formation of the orogenic curvature (b–c). (b): The initial compression created firstly a linear belt with a top-to-the WNW shearing sense, contemporaneous with pervasive SE-dipping schistosity, NW-directed thrust faults and asymmetrical folds above the décollement. (c): As the linear belt propagated toward the west, the Early Paleozoic batholiths acted as rigid blocks, and strain was thus transferred to the west of these batholiths and resulted in high strain ratios in the north and south sections. To the east of the batholiths, back-thrusting and folding provoked by batholith obstruction may be responsible for the tectonic uplifting of the Early Paleozoic rocks. (For interpretation of the references to colour in this figure legend, the reader is referred to the Web version of this article.)

7. Conclusion

The Xuefengshan Belt experienced intense intracontinental deformation in central South China, East Asia, dictating the structural mode and tectonic evolution during the Early Mesozoic. Quantitative strain analysis conducted throughout this belt reveals general strain patterns that allow us to draw several conclusions.

(1) The Xuefengshan Belt recorded generally intermediate to high strain, low temperature deformation that is dominated by a thrust-normal flattening mechanism during the westward propagation of the belt. The flattening strain pattern mirrors the prevailing effect of the schistosity-forming deformation (D_1), whereas minor constriction strain indicates later overprinting by D_2 and D_3.
(2) The strain field is heterogeneous in different structural positions. At basal levels, high strain was accumulated in metamorphic rocks near the décollement zone, as indicative of deformation localization. Low to intermediate strain ratios recorded in non-metamorphic rocks were closely related to the deformation style in high tectonic levels, where bulk strain was mostly accommodated by folding and thrusting.
(3) According to our strain data and field observation, deformation intensity and strain decrease from the east to the west, and drop significantly to the west of the Main Xuefengshan Belt, which marks the major boundary between the Western Zone and Eastern Zone of higher and lower tectonic levels, respectively. This variation corresponds well with the geometry and deformation.
(4) Along-strike variation with strain concentration along the North and South Sections is consistent with the development of the arcuate Xuefengshan Belt. During the fold-and-thrust belt propagation, large granitic batholiths that acted as stress barrier enhanced high strain accumulation to the west and tectonic imbrication to the east. In contrast, the Dongkou salient of the Middle Section migrated progressively to produce the final arcuate shape of the belt.

Acknowledgement

Field works have been supported by the Ministry of Science and Technology of the People's Republic of China (2016YFC0600401 and 2016YFC0600102), and the National Natural Science Foundation of China (418722208, 41472193, and 41302161). Dr. Dyanna Czeck and an anonymous reviewer are acknowledged for constructive comments and suggestions on this manuscript. Drs. Michel Faure and Yan Chen are acknowledged for discussion during the preparation of the manuscript. This work also benefited from fruitful discussion in Coffice-442, IGGCAS.

References

Avigad, D., Ziv, A., Garfunkel, Z., 2001. Ductile and brittle shortening, extension parallel folds and maintenance of crustal thickness in the central Aegean (Cyclades, Greece). Tectonics 20 (2), 277–287.
Bjørnerud, M.G., Boyer, B., 1996. Image analysis in structural geology using NIH Image. In: De Paor, D.G. (Ed.), Structural Geology and Personal Computers. Elsevier Science, Oxford, pp. 105–121.
Bureau of Geology and Mineral Resources of Guangxi province (BGMRGX), 1985. Regional Geology of the Guangxi Zhuang Autonomous Region. Geological Publishing House, Beijing, pp. 1–853.
Bureau of Geology and Mineral Resources of Hunan province (BGMRHN), 1988. Regional Geology of the Hunan Province. Geological Publishing House, Beijing, pp. 1–719.
Bureau of Geology and Mineral Resources of Jiangxi Province (BGMRJX), 1984. Regional Geology of the Jiangxi Province. Geological Publishing House, Beijing, pp. 1–921.
Charles, N., Faure, M., Chen, Y., 2009. The Montagne Noire migmatitic dome emplacement (French Massif Central): new insights from petrofabric and AMS studies. J. Struct. Geol. 31, 1423–1440.
Charvet, J., Shu, L.S., Shi, Y.S., Guo, L.Z., Faure, M., 1996. The building of south China: collision of Yangzi and Cathaysia blocks, problems and tentative answers. J. Southeast Asian Earth Sci. 13 (3–5), 223–235.
Charvet, J., et al., 2010. Structural development of the lower paleozoic belt of South China: genesis of an intracontinental orogen. J. Asian Earth Sci. 39 (4), 309–330.
Chew, D.M., 2003. An Excel spreadsheet for finite strain analysis using the Rf/φ technique. Comput. Geosci. 29, 795–799.

Chu, Y., Faure, M., Lin, W., Wang, Q., 2012a. Early mesozoic tectonics of the south China block: insights from the Xuefengshan intracontinental orogen. J. Asian Earth Sci. 61, 199–220.
Chu, Y., Faure, M., Lin, W., Wang, Q., Ji, W., 2012b. Tectonics of the Middle Triassic intracontinental Xuefengshan Belt, South China: new insights from structural and chronological constraints on the basal décollement zone. Int. J. Earth Sci. 101 (8), 2125–2150.
Chu, Y., Lin, W., Faure, M., Wang, Q., Ji, W., 2012c. Phanerozoic tectonothermal events of the Xuefengshan Belt, central South China: implications from U-Pb age and Lu-Hf determinations of granites. Lithos 150 (0), 243–255.
Chu, Y., Lin, W., 2014. Phanerozoic polyorogenic deformation in southern Jiuling Massif, northern South China block: constraints from structural analysis and geochronology. J. Asian Earth Sci. 86, 117–130.
Chu, Y., Lin, W., Faure, M., Wang, Q., 2015. Early mesozoic intracontinental orogeny: example of the Xuefengshan-Jiuling belt. Acta Petrol. Sin. 31 (8), 2145–2155 (in Chinese with English abstract).
Coward, M.P., Kim, J.H., 1981. Strain within thrust sheets. Geo. Soc. Lond. Spec. Publ. 9, 275–292.
Czeck, D.M., Fissler, D.A., Horsman, E., Tikoff, B., 2009. Strain analysis and rheology contrasts in polymictic conglomerates: an example from the Seine metaconglomerates, Superior Province, Canada. J. Struct. Geol. 31, 1365–1376.
Dunnet, D., 1969. A technique of finite strain analysis using elliptical particles. Tectonophysics 7, 117–136.
Erslev, E.A., 1988. Normalized center-to-center strain analysis of packed aggregates. J. Struct. Geol. 10 (2), 201–209.
Faure, M., Sun, Y., Shu, L., Moni, P., Charvet, J., 1996. Extensional tectonics within a subduction-type orogen. The case study of the Wugongshan dome (Jiangxi Province, southeastern China). Tectonophysics 263, 77–106.
Faure, M., Lin, W., Shu, L.S., Sun, Y., Scharer, U., 1999. Tectonics of the Dabieshan (eastern China) and possible exhumation mechanism of ultra high-pressure rocks. Terra. Nova 11 (6), 251–258.
Faure, M., Shu, L., Wang, B., Charvet, J., Choulet, F., Monie, P., 2009. Intracontinental subduction: a possible mechanism for the early palaeozoic orogen of SE China. Terra. Nova 21 (5), 360–368.
Hacker, B.R., Ratschbacher, L., Webb, L., Ireland, T., Walker, D., Shuwen, D., 1998. U/Pb zircon ages constrain the architecture of the ultrahigh-pressure Qinling-Dabie Orogen, China. Earth Planet Sci. Lett. 161 (1–4), 215–230.
Hartz, E.H., Andresen, A., 1997. From collision to collapse: complex strain permutations in the hinterland of the Scandinavian Caledonides. J. Geophys. Res. 102 (24) 697e724. 712.
Kenis, I., Urai, J., Vanderzee, W., Hilgers, C., Sintubin, M., 2005. Rheology of fine-grained siliciclastic rocks in the middle crust—evidence from structural and numerical analysis. Earth Planet Sci. Lett. 233 (3–4), 351–360.
Kirkland, C.L., Daly, J.S., Eide, E.A., Whitehouse, M.J., 2006. The structure and timing of lateral escape during the Scandian Orogeny: a combined strain and geochronological investigation in Finnmark, Arctic Norwegian Caledonides. Tectonophysics 425 (1–4), 159–189.
Law, R.D., Searle, M.P., Simpson, R., 2004. Strain, deformation temperatures and vorticity of flow at the top of the greater Himalayan slab, everest massif, Tibet. J. Geol. Soc. 161, 305–320.
Lepvrier, C., Maluski, H., Van Tich, V., Leyreloup, A., Truong Thi, P., Van Vuong, N., 2004. The early Triassic Indosinian orogeny in Vietnam (Truong Son belt and Kontum massif); implications for the geodynamic evolution of Indochina. Tectonophysics 393, 87–118.
Li, J., Dong, S., Zhang, Y., Zhao, G., Johnston, S.T., Cui, J., Xin, Y., 2016. New insights into Phanerozoic tectonics of south China: Part 1, polyphase deformation in the Jiuling and Lianyunshan domains of the central Jiangnan Orogen. J. Geophys. Res.: Solid Earth 121, 3048–3080.
Li, X.H., Li, Z.X., Ge, W.C., Zhou, H.W., Li, W.X., Liu, Y., Wingate, M.T.D., 2003. Neoproterozoic granitoids in South China: crustal melting above a mantle plume at ca. 825 Ma? Precambrian Res. 122 (1–4), 45–83.
Li, Z.X., Li, X.H., 2007. Formation of the 1300-km-wide intracontinental orogen and postorogenic magmatic province in Mesozoic South China: a flat-slab subduction model. Geology 35, 179–182.
Li, Z.X., Li, X.H., Wartho, J.A., Clark, C., Li, W.X., Zhang, C.L., Bao, C., 2010. Magmatic and metamorphic events during the early Paleozoic Wuyi-Yunkai orogeny, southeastern South China: new age constraints and pressure-temperature conditions. Geol. Soc. Am. Bull. 122, 772–793.
Lisle, R.J., 1985. Geological Strain Analysis: a Manual for the R_f-φ Technique. Pergamon Press, Oxford.
Long, S., McQuarrie, N., Tobgay, T., Hawthorne, J., 2011. Quantifying internal strain and deformation temperature in the eastern Himalaya, Bhutan: implications for the evolution of strain in thrust sheets. J. Struct. Geol. 33, 579–608.
McLeish, A.J., 1971. Strain analysis of deformed pipe rock in the moine thrust zone, northwest Scotland. Tectonophysics 12, 469–503.
Means, W.D., 1994. Rotational quantities in homogeneous flow and the development of smallscale structure. J. Struct. Geol. 16, 437–445.
Means, W.D., Hobbs, B.E., Lister, G.S., Williams, P.F., 1980. Vorticity and non-coaxiality in progressive deformations. J. Struct. Geol. 2, 371–378.
Mitra, G., 1994. Strain variation in thrust sheets across the sevier fold-and-thrust belt (Idaho-Utah-Wyoming): implications for section restoration and wedge taper evolution. J. Struct. Geol. 16 (4), 585–602.
Mukul, M., Mitra, G., 1998. Finite strain and strain variation analysis in the Sheeprock Thrust Sheet: an internal thrust sheet in the Provo salient of the Sevier Fold-and-Thrust belt, Central Utah. J. Struct. Geol. 20 (4), 385–405.
Okudaira, T., Beppu, Y., 2008. Inhomogeneous deformation of metamorphic tectonites of contrasting lithologies: strain analysis of metapelite and metachert from the Ryoke metamorphic belt, SW Japan. J. Struct. Geol. 30, 39–49.
Okudaira, T., Beppu, Y., Yano, R., Tsuyama, M., Ishii, K., 2009. Mid-crustal horizontal shear zone in the forearc region of the mid-Cretaceous SW Japan arc, inferred from strain analysis of rocks within the Ryoke metamorphic belt. J. Asian Earth Sci. 35, 34–44.
Qiu, Y.X., Zhang, Y.C., Ma, W.P., 1998. Tectonics and geological evolution of Xuefeng intra-continental orogen, south China (in Chinese with English abstract). Geol. J. China Univ. 4 (4), 432–443.
Ramsay, J.G., 1967. Folding and Fracturing of Rocks. McGraw-Hill, New York.
Ramsay, J.G., Huber, M.I., 1983. The techniques of modern structural geology. Strain Analysis, vol. 1 Academic Press.
Robin, P.F., Torrance, F.G., 1987. Statistical analysis of the effect of sample size on paleostrain calculation. I. Single face measurements. Tectonophysics 138, 311–317.
Shu, L., Charvet, J., 1996. Kinematics and geochronology of the Proterozoic Dongxiang-Shexian ductile shear zone: with HP metamorphism and ophiolitic melange (Jiangnan Region, South China). Tectonophysics 267 (1–4), 291–302.
Shu, L.S., Zhou, X.M., Deng, P., Wang, B., Jiang, S.Y., Yu, J.H., Zhao, X.X., 2009. Mesozoic tectonic evolution of the Southeast China Block: new insights from basin analysis. J. Asian Earth Sci. 34, 376–391.
Treagus, S.H., Treagus, J.E., 2002. Studies of strain and rheology of conglomerates. J. Struct. Geol. 24, 1541–1567.
Tull, J.F., Baggazi, H., Groszos, M.S., 2012. Evolution of the murphy synclinorium, southern Appalachian Blue ridge, USA. J. Struct. Geol. 44, 151–166.
Wang, J., Li, Z.X., 2003. History of Neoproterozoic rift basins in South China: implications for Rodinia break-up. Precambrian Res. 122 (1–4), 141–158.
Wang, W., Chen, F., Hu, R., Chu, Y., Yang, Y.-Z., 2012. Provenance and tectonic setting of Neoproterozoic sedimentary sequences in the South China Block: evidence from detrital zircon ages and Hf–Nd isotopes. Int. J. Earth Sci. 101, 1723–1744.
Wang, W., Zhou, M.F., Yan, D.P., Li, L., Malpas, J., 2013. Detrital zircon record of Neoproterozoic active-margin sedimentation in the eastern Jiangnan Orogen, South China. Precambrian Res. 235, 1–19.
Wang, Y.J., Zhang, Y.H., Fan, W.M., Peng, T.P., 2005. Structural signatures and Ar-40/Ar-39 geochronology of the Indosinian Xuefengshan tectonic belt, south China block. J. Struct. Geol. 27 (6), 985–998.
Weil, A.B., Sussman, A.J., 2004. Classifying curved orogens based on timing relationships between structural development and vertical-axis rotations. Geol. Soc. Am. Spec. Pap. 383, 1–15.
Yan, D.P., Zhou, M.F., Song, H.L., Wang, X.W., Malpas, J., 2003. Origin and tectonic significance of a mesozoic multi-layer over-thrust system within the Yangtze block (south China). Tectonophysics 361, 239–254.
Yan, D.P., Zhou, M.F., Li, S.B., Wei, G.Q., 2011. Structural and geochronological constraints on the Mesozoic-Cenozoic tectonic evolution of the Longmen Shan thrust belt, eastern Tibetan Plateau. Tectonics 30https://doi.org/10.1029/2011TC002867. TC6005.
Yonkee, A., 2005. Strain patterns within part of the Willard thrust sheet, Idaho–Utah–Wyoming thrust belt. J. Struct. Geol. 27, 1315–1343.
Yonkee, A., Weil, A.B., 2010. Reconstructing the kinematic evolution of curved mountain belts: Internal strain patterns in the Wyoming salient, Sevier thrust belt, U.S.A. Geol. Soc. Am. Bull. 122, 24–49.
Yonkee, W.A., Czeck, D.M., Nachbor, A.C., Barszewski, C., Pantone, S., Balgord, E.A., Johnson, K.R., 2013. Strain accumulation and fluid–rock interaction in a naturally deformed diamictite, Willard thrust system, Utah (USA): Implications for crustal rheology and strain softening. J. Struct. Geol. 50, 91–118.
Zhang, S., Jiang, G., Zhang, J., Song, B., Kennedy, M.J., Christie-Blick, N., 2005. U-Pb sensitive high-resolution ion microprobe ages from the Doushantuo Formation in south China: Constraints on late Neoproterozoic glaciations. Geology 33 (6), 473–476.